

# Altermagnetic polarons

Maria Daghofer,<sup>1,\*</sup> Krzysztof Wohlfeld,<sup>2</sup> and Jeroen van den Brink<sup>3,4</sup>

<sup>1</sup>*Institut für Funktionelle Materie und Quantentechnologien, Universität Stuttgart, 70550 Stuttgart, Germany*

<sup>2</sup>*Institute of Theoretical Physics, Faculty of Physics, University of Warsaw, Pasteura 5, PL-02093 Warsaw, Poland*

<sup>3</sup>*Leibniz-Institut für Festkörper- und Werkstoffforschung, Helmholtzstraße 20, D-01069 Dresden, Germany*

<sup>4</sup>*Institute of Theoretical Physics and Würzburg-Dresden Cluster of Excellence ct.qmat, Technische Universität Dresden, 01062 Dresden, Germany*

(Dated: June 11, 2025)

While a spin-dependent band-splitting is one of the characteristic features of altermagnets, the conventional band-picture itself breaks down in the many altermagnets that are correlated Mott materials. We employ two numerical many-body methods, the self-consistent Born approximation and variational cluster approach, to explore this strongly correlated regime and investigate hole motion in Mott altermagnets. Our results reveal that spin-dependent spectral-weight transfer is the dominant signature of Mott altermagnetism. This pronounced spin-momentum locking of the quasiparticle spectral weight arises from the formation of altermagnetic polarons, whose dynamics are governed by the interplay between free hole motion and the coupling of the hole to magnon excitations in the altermagnet. We demonstrate this effect by calculating ARPES spectra for two canonical altermagnetic systems: the checkerboard  $J$ - $J'$  model and the Kugel-Khomskii spin-orbital altermagnet based on cubic vanadates  $RVO_3$  ( $R$ =La, Pr, Nd, Y).

It was recently discovered that, depending on their symmetries, collinear antiferromagnets may break spin degeneracy in momentum space, even in the absence of spin-orbit coupling, giving rise to a set of magnetic materials referred to as altermagnets (AMs) [1–6]. At a single-particle level, valid for systems with weak electron-electron interactions, this gives rise to electronic bands with anisotropic, spin-split iso-energy surfaces. The anisotropic bands in turn lead to a series of unusual electric, magneto-electric and optical properties [7–9]. Indeed, such spin-split bands corresponding to (very) weak correlations without band renormalization have been observed in angle-resolved photoemission (ARPES) experiments, for instance in metallic CrSb or semiconducting MnTe [10–16].

However, a large set of AMs are actually strongly correlated Mott insulators, with band gaps determined by the Hubbard electron-electron interaction [6]. This comprises, e.g., a series of transition metal fluoride AMs with rutile structure [6], vanadates [17], or the recently discovered layered AM  $La_2O_3Mn_2Se_2$  [18]. It is well known that in canonical correlated antiferromagnets the band-picture fails as many-body effects strongly renormalize quasiparticle dispersions all the way down to the magnetic energy scale, and at the same time vehemently reorganize spectral weights (SWs) [19, 20]. This raises the question as to the fate of altermagnets and their dynamical properties in the strongly correlated and Mott insulating regime.

In strong-coupling correlated antiferromagnets the large difference with the bare single-particle electronic dispersions is due to the disruptions in the antiferromagnetic (AF) background that are caused by a moving charge carrier. Its motion dynamically creates and annihilates excitations of the AF background, usually magnons, and the interplay of hole and magnons strongly modifies hole propagation. While a quasi-particle (QP) – the spin polaron – often survives, it contains only part of the SW and has a dispersion of the order of the magnetic exchange  $J$  rather than of the bare hopping

$t$  [21]. The missing weight is lost into an incoherent continuum [1, 22] that is usually separated from the polaronic QP band and distributed over a width  $\propto t$ . The description of charge carriers in terms of spin polarons in antiferromagnets is widely used [24–26] to interpret ARPES measurements on cuprates [27, 28] and has been extended to describe orbital excitations in iridates [29] and cuprates [30], as well as been investigated in ultracold-atom quantum simulators [31–33]. Certain theoretical aspects of AMs beyond the weak-coupling regime have been considered, in particular the existence of lower and upper Hubbard bands in addition to altermagnetic band splitting [34] and the persistence of altermagnetic signatures into a frustrated and/or fluctuating regime [35, 36]. However, the impact of altermagnetic symmetries on the properties of strongly interacting quasi-particles and spin polarons, which are directly related to the spectral function measured in ARPES, have not been considered so far.

Here we consider the correlated charge propagation in Mott-insulating altermagnets, i.e. the spin polaron in an altermagnet instead of an antiferromagnet. Both the bare dispersion, which one would observe without correlations, and the magnon spectrum [37, 38], which strongly modifies the effective dispersion of a spin polaron, have momentum-dependent band splittings in altermagnets that are not present in antiferromagnets. Focusing on a  $t$ - $J$  model on the checkerboard lattice, we find that momentum and spin of the polaron are similarly strongly linked. However, in contrast to weakly interacting altermagnets, this is not necessarily reflected in a band splitting, but rather in the particle life time: One spin projection is pushed into the incoherent spectrum, losing its quasi-particle character, so that the surviving quasi-particle shows spin-momentum locking.

We also look at hole motion in a Mott-insulating Kugel-Khomskii-type model for layered vanadates of the form  $RVO_3$  ( $R$ =La, Pr, Nd, Y) that combine three-dimensional orbital and magnetic order [39–41]. Orbital order is driven by a combina-

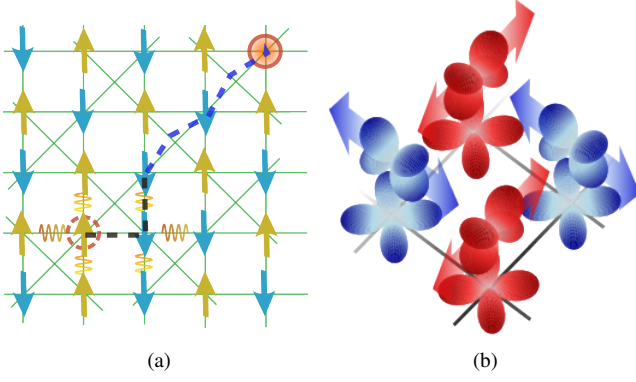


FIG. 1. (a) cartoon for hole propagation in the checkerboard model: The hole has moved from its original position (dashed empty circle) to the current one (filled circle) via two NN hoppings (black dashed horizontal and vertical line) and two NNN hopping processes (blue diagonal lines). The NN processes have disturbed the AF background and thus created magnons, the NNN hopping left it intact. (b) Cartoon for the spin-orbital model based on  $\text{LaVO}_3$ . The  $xy$  orbital is half filled and superexchange leads to AF order, indicated by red and blue color. Additionally, the  $xz/yz$  orbitals share one electron, which can only hop along one direction and whose spin is aligned to the  $xy$  spin on the same site.

tion of lattice and superexchange effects, with  $\text{LaVO}_3$  being most clearly dominated by superexchange [41]. Looking at a single two-dimensional plane, spin and orbital alternate together in an antiferromagnetic/antiferroorbital (AF/AO) pattern as sketched in Fig. 1(b), suggesting an AM state [42]. In fact, band-structure calculations have found  $\text{YVO}_3$  to be an altermagnet [17], and we will show that holes are then expected to move as altermagnetic polarons.

*Spectral function of the checkerboard altermagnetic polaron* — Our considerations start from a  $t$ - $J$  model on the checkerboard lattice (see Fig. 1a) defined by

$$H = -t \sum_{\langle i,j \rangle, \sigma} c_{i,\sigma}^\dagger c_{j,\sigma} - t' \sum_{\langle\langle i,j \rangle\rangle \parallel (1,1)} c_{i,\sigma}^\dagger c_{j,\sigma} - t' \sum_{\langle\langle i,j \rangle\rangle \parallel (1,-1)} c_{i,\sigma}^\dagger c_{j,\sigma} \quad (1)$$

$$+ J \sum_{\langle i,j \rangle} \mathbf{S}_i \mathbf{S}_j + J' \sum_{\langle\langle i,j \rangle\rangle \parallel (1,1)} \mathbf{S}_i \mathbf{S}_j + J' \sum_{\langle\langle i,j \rangle\rangle \parallel (1,-1)} \mathbf{S}_i \mathbf{S}_j, \quad (2)$$

where  $c_{i,\sigma}^\dagger$  ( $c_{i,\sigma}$ ) creates (annihilates) an electron with spin  $\sigma = \uparrow, \downarrow$  on site  $i$ .  $\mathbf{S}_i$  denotes the corresponding vector of spin operators  $S_i^\alpha = \frac{1}{2} \sum_{s,s'} c_{i,s}^\dagger \sigma_{s,s'}^\alpha c_{i,s'}$  with Pauli matrices  $\sigma^\alpha$ . Nearest-neighbor (NN) bonds  $\langle i, j \rangle$  connect the two sublattices  $A$  and  $B$ . Bonds  $\langle\langle i, j \rangle\rangle$  connect sites from the same sublattice and are active only along direction  $(1, 1)$  for the  $A$  sublattice and  $(1, -1)$  for  $B$ , see Fig. 1(a). NN hopping  $t$  is used as unit of energy.

We employ the self-consistent Born approximation (SCBA) [21] by largely following Refs. [43–45] to obtain the Green's function of the spin-polaron in the half-filled AM ordered state, which provides the one-particle spectral density.

The spin-part (2) of the Hamiltonian becomes

$$\tilde{H}_J = \omega_{\alpha,\mathbf{k}} \alpha_{\mathbf{k}}^\dagger \alpha_{\mathbf{k}} + \omega_{\beta,\mathbf{k}} \beta_{\mathbf{k}}^\dagger \beta_{\mathbf{k}}, \quad (3)$$

where  $\alpha_{\mathbf{k}}^\dagger$  ( $\alpha_{\mathbf{k}}$ ) and  $\beta_{\mathbf{k}}^\dagger$  ( $\beta_{\mathbf{k}}$ ) create (annihilate) magnons of the two branches, see [46] for more details as well as the derived expression for the kinetic part (1).

The primary advantage of SCBA is that it very accurately captures the unavoidable coupling between the hole and the collective excitations from the ordered state—the magnons (see SM [46] for more details). More precisely, the NN hole hopping between sublattices always creates or annihilates magnons and thus couples hole motion and magnons, see Fig. 1(a). It is then only the subdominant NNN hole hopping within a sublattice that does not disturb the AM background, see Fig. 1(a). The SCBA captures both of these processes in the self-consistent equations for the self energy

$$\Sigma^\alpha(\mathbf{k}, \omega) = \frac{z^2 t^2}{N_u} \sum_{\mathbf{k}'} M_{\mathbf{k},\mathbf{k}'}^2 G^{\bar{\alpha}}(\mathbf{k} - \mathbf{k}', \omega - \omega_{\bar{\alpha},\mathbf{k}'}) , \quad (4)$$

for sublattice  $\alpha = A, B$ . As NN hopping changes sublattice, the Green's function  $G^{\bar{\alpha}}$  entering the sum is the one of the opposite sublattice  $\bar{\alpha} = B, A$  and the energy difference  $\omega_{\bar{\alpha},\mathbf{k}'}$  is the energy of the emitted and re-absorbed  $\alpha$ - ( $\beta$ -) magnon for  $\Sigma^B$  ( $\Sigma^A$ ). The vertex  $M_{\mathbf{k},\mathbf{k}'}$  is given in the SM [46],  $z = 4$  is the coordination number and  $N_u$  the number of unit cells. The Green's function of obtained from the self energy via the Dyson equation

$$[G^\alpha(\mathbf{k}, \omega)]^{-1} = \omega - \epsilon^\alpha(\mathbf{k}) - \Sigma^\alpha(\mathbf{k}, \omega) + i\delta, \quad (5)$$

with the free dispersion  $\epsilon^\alpha(\mathbf{k}) = 2t' \cos k_\alpha$  coming from NNN hopping. Higher-order processes are here effectively included, as long as they do not contain crossing magnon lines. For square-lattice AF states, the lowest crossing terms vanish, and the impact of the non-crossing approximation has been found to be negligible [47].

While quantum fluctuations imply that spin is not perfectly tied to sublattice [46], resulting one-particle spectra remain clearly spin dependent, as can be seen in Fig. 2 for  $J' = 0.15 t$  and  $t' = -0.5 t$ . On the checkerboard lattice, altermagnetic signatures can be expected to be most pronounced at momenta  $(\frac{\pi}{2}, \pm \frac{\pi}{2})$ , emphasized with blue and red lines in Fig. 2. However, the spectra do not show a splitting between an 'up'-band and a 'down'-band as in weak-coupling spectra, but rather a single coherent QP with momentum-dependent spin polarization. The opposite spin is largely smeared out into the incoherent weight at higher excitation energies.

How does this spin-dependent splitting into QP vs. continuum connect to the AF case, where there is of course one QP for each spin, and both are degenerate? The high-resolution spectrum for  $J' = 0.15 t$  and rather small  $t' = 0.1 t$  in Fig. 3(a) indeed shows two spin-polarized bands with an energy splitting reminiscent of weak-coupling altermagnets. However, the spin-down band is already very close to the next (continuum) states, even though the energy difference between the

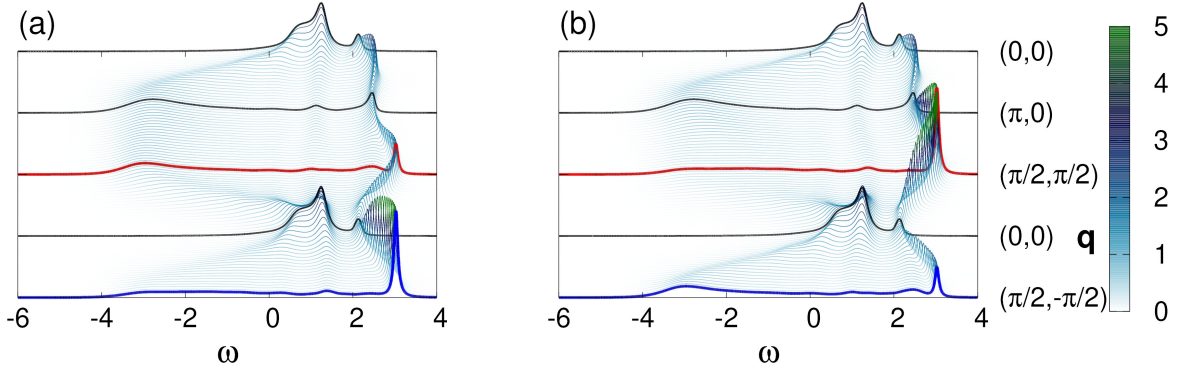


FIG. 2. One-particle spectral density obtained with SCBA for the checkerboard model with  $J = 0.4 t$ , NNN  $J' = 0.15 t$  and  $t' = -0.5 t$  and (a) spin up, (b) spin down. Momenta are here given in terms of a one-site unit cell; peaks were broadened with a Lorentzian of width  $0.05 t$  for plotting. For comparison to the usual square-lattice antiferromagnet, momenta  $\mathbf{q}$  here correspond to a one-site unit cell. They can be obtained from momenta  $\mathbf{k}$  of the two-site unit cell as  $q_{x/y} = (k_a \pm k_b)/2$ .

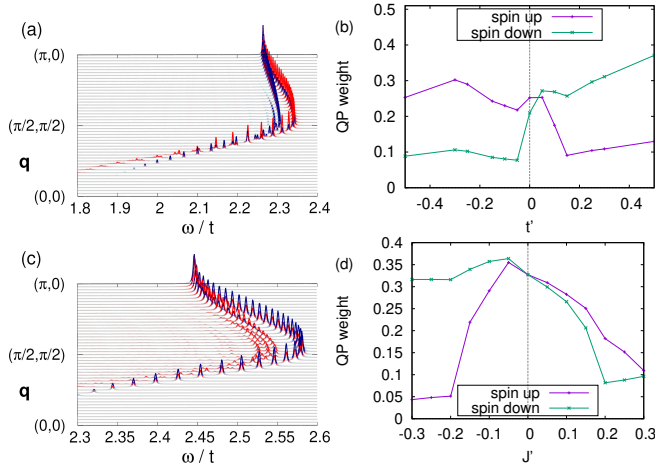


FIG. 3. (a) and (c) give high-resolution spectra for spin up (red) and down (blue) and parameters (a)  $J' = 0.15 t$ ,  $t' = 0.1 t$  and (c)  $J' = 0.25 t$ ,  $t' = 0$ . (b) and (d) give QP weights at momentum  $(\frac{\pi}{2}, \frac{\pi}{2})$  for (b)  $J' = 0.15 t$  and variable  $t'$  and (d)  $t' = 0$  and variable  $J'$ . The QP part of the spectrum always includes the lowest-energy excitation, which is the highest peak and well separated from remaining features for all parameter sets. For some parameter sets near the AF point, a second peak (of opposite spin polarization to the first) is also separated from the remaining spectrum, it was then included into the QP weight. The criterion to distinguish this second QP peak was whether it is larger than the third peak.

bands is very small. Figure 3(b) illustrates that the regime with two QPs is confined to  $t' \approx 0$ , and one QP is quickly lost into the continuum.

The altermagnetic coupling  $J'$  has a much weaker effect on the bands than the AM hopping  $t'$ , so that two QPs can be found up to quite substantial values of  $|J'| \lesssim 0.2 t = 2J/3$ , see Fig. 3(d). For  $J' = 0.25 t$ , one QP has merged into the continuum, see Fig. 3(c). However, weight remains concentrated near the top of the continuum and energy distance to the QP peak is small, so that lower resolution might easily mask the impact of even this large  $J'$ . Close to the breakdown of

Néel magnetic order for large  $J' > 0$ , quantum fluctuations additionally reduce spin polarization of spectral features, including the QP, see Fig. 3(d).

To cross-check these findings and establish their physical pertinence we have complemented the SCBA study with the variational cluster approximation (VCA) [2] applied to a Hubbard-model variant of the checkerboard model. The  $J$  and  $J'$  terms of (2) are here replaced by an onsite Hubbard repulsion  $U \sum_i n_{i,\uparrow} n_{i,\downarrow}$ . We choose  $U = 10 t$  which gives an effective NN superexchange  $J = \frac{4t^2}{U} = 0.4 t$  as before, and puts us solidly in the Mott insulating regime at half filling. Further setting  $t' = \pm 0.2 t$  and  $\pm 0.5 t$ , we then verified [46] that the magnetically ordered state has a QP with momentum-dependent spin polarization, analogous to the SCBA spectra discussed in Fig. 2 above.

Spin-dependent weight transfer is not unique to the checkerboard lattice, as we find by applying the VCA to the Hubbard model on the Shastry-Sutherland lattice [46], where signatures of altermagnetism were previously studied with variational wave functions [35]. We find that one-particle spectra are generally less coherent than for the checkerboard model, especially for stronger frustration [46]. Nevertheless, the most coherent QP-like features again show spin-momentum locking, with the 'missing' spin being pushed into the incoherent spectrum.

*Altermagnetic polaron spectral function in  $\text{LaVO}_3$*  — To establish a platform where the altermagnetic polaron can be experimentally identified and investigated, we consider a three-orbital model relevant for  $\text{LaVO}_3$ . We thus apply the VCA to a three-orbital  $t_{2g}$  model with kinetic energy

$$H_{t_{2g}} = -t \sum_{\langle i,j \rangle, \sigma} c_{i,xy,\sigma}^\dagger c_{j,xy,\sigma} + \Delta \sum_{i,\sigma} n_{i,xy,\sigma} \quad (6)$$

$$-t \sum_{\langle i,j \rangle \parallel a, \sigma} c_{i,xz,\sigma}^\dagger c_{j,xz,\sigma} - t \sum_{\langle i,j \rangle \parallel b, \sigma} c_{i,yz,\sigma}^\dagger c_{j,yz,\sigma} \quad (7)$$

on the square lattice, where  $c_{i,\alpha,\sigma}^\dagger$  refers to an electron with spin  $\sigma$  in orbital  $\alpha$  on site  $i$ . The dominant energy scale is here onsite interaction  $U$  together with Hund's-rule coupling,



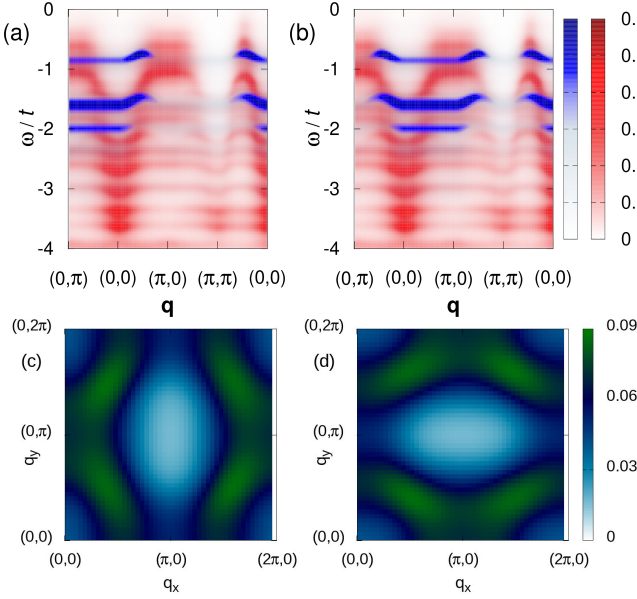


FIG. 4. Occupied states obtained with VCA for the three-orbital  $t_{2g}$  model with  $t = 1$ ,  $U = 14t$ ,  $J_H = 2t$ ,  $\Delta = -0.5t$  in the AF and AO state illustrated in Fig. 1(b). (a) gives the energy- and momentum dependent spectrum for spin up and (b) for spin down. Weight in red comes from the  $xy$  orbital, while the combined  $xz$  and  $yz$  weight is shown in blue, however, this corresponds to mostly  $xz$  and  $yz$  character resp. (c) and (d) show the weight of up. resp. down states integrated over the energy range  $-1.2t < \omega < -0.5t$ , all orbitals.

see [46], so that a filling of two electrons corresponds to a Mott insulator with large spin one. Crystal field splitting  $\Delta < 0$  ensures that one electron is found in the  $xy$  orbital, and this half-filled  $xy$  orbital strongly promotes AF magnetic order. The second electron can be in either the  $xz$  or the  $yz$  state and the VCA here finds the AF/AO order of Fig. 1(b) to be favorable.

In general orbital order has a strong Ising-like – rather than Heisenberg-like – character, and in the AF/AO state this Ising character is also imparted onto the spin degree of freedom [45]. The VCA spectra for the AF/AO state are shown in Fig. 4 and show the QP peaks with spin-dependent dispersion expected from earlier work [45]. Hole motion is almost completely driven by three-site hopping of the hole [44, 49] that acts along the  $x$ -( $y$ )-axis for a hole inserted into the  $xz$  ( $yz$ ) orbital. As spin and orbitals are ‘locked’ together by the AO/AF order, a hole inserted into a particular orbital also has a definite spin polarization. The spin-dependent dispersion is then mirrored in a few replica bands with increasing excitation energy (‘the ladder spectrum’), which are due to the polaronic motion in an Ising-like AO/AF state.

In addition to spin-dependent dispersion, however, we also find substantial spin-dependent SW transfer—see spectra at the special AM momenta as well as the integrated SW in Fig. 4(c) and (d): Spectra around momenta  $\mathbf{q} = (\pi, 0)$  and  $(0, \pi)$  are strongly spin polarized, especially within the combined  $xz/yz$  sector. SW is here not transferred into higher-

energy incoherent features, all peaks of the ladder spectrum in contrast have a similar weight distribution. Instead, the missing weight of opposite spin is located in the upper Hubbard band, a many-body effect that is due to the interplay between polaronic and free holon motion. Spin polarization is somewhat diluted by the  $xy$  orbital, where a hole sees ferro-orbital order and can hop in both directions; the  $xy$  weight in Fig. 4 is consequently two-dimensional as well as identical for both spins.

*Conclusions and outlook* — We have here extended the discussion of altermagnetic symmetries to the strong-coupling case of a spin polaron formed by hole in altermagnetic Mott insulators and which also are applicable to newly designed spin-cluster altermagnets realized from strongly-correlated building blocks [50]. Spin-split QP peaks of both spin species may be preserved if they are well separated from the rest of the spectrum, as in the Ising-like case of spin-orbital order in a  $t_{2g}$ -model based on  $\text{LaVO}_3$ . Weights of the two QPs are however generally quite different, resulting in effective spin-momentum locking. In an AM with Heisenberg spin-spin coupling, a single QP peak with clear spin-momentum locking is typical, while the spectral weight of opposite spin is incoherent and broad.

The effect of altermagnetic band splitting on superconductivity has already become an extensive area of research. For instance, the band splitting can give Cooper pairs a finite momentum even without a magnetic field [51, 52], or one may think of a superconducting diode effect [53]. Moreover, the Lieb lattice formed by Cu and O ions in cuprate superconductors can form an AM [54]. In this context our findings raise the question of what happens when stronger correlations not only shift the band energies, but instead render bands of one spin species incoherent, as we find here to happen in a spin background with quantum fluctuations.

This point immediately relates to a longstanding debate in the field of high-temperature superconductors on pairing mediated by correlations [55]. The spin polaron suppresses spin order in the vicinity of the mobile charge, which self-consistently traps the charge [56]. This so-called spin bag does not carry a spin in antiferromagnets, but from our results it is clear that in altermagnets it does. As electrons sharing a common bag mediates pairing, it will be interesting to establish how this affects the pairing between altermagnetic quasiparticles of opposite momentum. Very recently, numerical studies of the square-lattice Hubbard model have addressed the relative importance of pairing mechanisms due to spin fluctuations vs. others based more directly on short-range interactions [57–59]. The difference between AM and AF states when it comes to polaron spin and spin-momentum locking suggest that numerical (and potentially experimental) investigations of superconductivity in strongly correlated altermagnets could also contribute further insights.

*Acknowledgments* — K.W. thanks National Science Center, Poland for financial support (grant number 2024/55/B/ST3/03144). Part of this work was supported by the Deutsche Forschungsgemeinschaft (DFG, German

Research Foundation) through the Sonderforschungsbereich SFB 1143, grant No. YE 232/2-1, and under Germany's Excellence Strategy through the Würzburg-Dresden Cluster of Excellence on Complexity and Topology in Quantum Matter – *ct.qmat* (EXC 2147, project-ids 390858490 and 392019).

*Note added*— While working on this manuscript, we became aware of work by L. Lanzini *et al.* discussing related issues [60].

- 
- [1] L. Šmejkal, R. González-Hernández, T. Jungwirth, and J. Sinova, Crystal time-reversal symmetry breaking and spontaneous hall effect in collinear antiferromagnets, *Science Advances* **6**, eaaz8809 (2020).
- [2] L. Šmejkal, J. Sinova, and T. Jungwirth, Emerging research landscape of altermagnetism, *Phys. Rev. X* **12**, 040501 (2022).
- [3] M. Naka, S. Hayami, H. Kusunose, Y. Yanagi, Y. Motome, and H. Seo, Spin current generation in organic antiferromagnets, *Nature Communications* **10**, 4305 (2019).
- [4] L.-D. Yuan, Z. Wang, J.-W. Luo, E. I. Rashba, and A. Zunger, Giant momentum-dependent spin splitting in centrosymmetric low-Z antiferromagnets, *Phys. Rev. B* **102**, 014422 (2020).
- [5] M. Naka, Y. Motome, and H. Seo, Perovskite as a spin current generator, *Phys. Rev. B* **103**, 125114 (2021).
- [6] Y. Guo, H. Liu, O. Janson, I. C. Fulga, J. van den Brink, and J. I. Facio, Spin-split collinear antiferromagnets: A large-scale ab-initio study, *Materials Today Physics* **32**, 100991 (2023).
- [7] L. Šmejkal, A. H. MacDonald, J. Sinova, S. Nakatsuji, and T. Jungwirth, Anomalous Hall antiferromagnets, *Nature Reviews Materials*, 2058 (2022).
- [8] T. Sato, S. Haddad, I. C. Fulga, F. F. Assaad, and J. van den Brink, Altermagnetic anomalous hall effect emerging from electronic correlations, *Phys. Rev. Lett.* **133**, 086503 (2024).
- [9] P. A. McClarty and J. G. Rau, Landau theory of altermagnetism, *Phys. Rev. Lett.* **132**, 176702 (2024).
- [10] S. Reimers, L. Odenbreit, L. Šmejkal, V. N. Strocov, P. Constantinou, A. B. Hellenes, R. Jaeschke Ubierno, W. H. Campos, V. K. Bharadwaj, A. Chakraborty, T. Denneulin, W. Shi, R. E. Dunin-Borkowski, S. Das, M. Kläui, J. Sinova, and M. Jourdan, Direct observation of altermagnetic band splitting in CrSb thin films, *Nature Communications* **15**, 10.1038/s41467-024-46476-5 (2024).
- [11] G. Yang, Z. Li, S. Yang, J. Li, H. Zheng, W. Zhu, Z. Pan, Y. Xu, S. Cao, W. Zhao, A. Jana, J. Zhang, M. Ye, Y. Song, L.-H. Hu, L. Yang, J. Fujii, I. Vobornik, M. Shi, H. Yuan, Y. Zhang, Y. Xu, and Y. Liu, Three-dimensional mapping of the altermagnetic spin splitting in CrSb, *Nature Communications* **16**, 1442 (2025).
- [12] M. Zeng, M. Zhu, Y. Zhu, X. Liu, X. Ma, Y. Hao, P. Liu, G. Qu, Y. Yang, Z. Jiang, K. Yamagami, M. Arita, X. Zhang, T. Shao, Y. Dai, K. Shimada, Z. Liu, M. Ye, Y. Huang, Q. Liu, and C. Liu, Observation of spin splitting in room-temperature metallic antiferromagnet CrSb, *Advanced Science* **11**, 2406529 (2024).
- [13] J. Ding, Z. Jiang, X. Chen, Z. Tao, Z. Liu, T. Li, J. Liu, J. Sun, J. Cheng, J. Liu, Y. Yang, R. Zhang, L. Deng, W. Jing, Y. Huang, Y. Shi, M. Ye, S. Qiao, Y. Wang, Y. Guo, D. Feng, and D. Shen, Large band splitting in *g*-wave altermagnet CrSb, *Phys. Rev. Lett.* **133**, 206401 (2024).
- [14] C. Li, M. Hu, Z. Li, Y. Wang, W. Chen, B. Thiagarajan, M. Leandersson, C. Polley, T. Kim, H. Liu, C. Fulga, M. G. Vergniory, O. Janson, O. Tjernberg, and J. van den Brink, *Topological weyl altermagnetism in CrSb* (2024), [arXiv:2405.14777 \[cond-mat.mtrl-sci\]](https://arxiv.org/abs/2405.14777).
- [15] J. Krempaský, L. Šmejkal, S. W. D'Souza, M. Hajlaoui, G. Springholz, K. Uhlířová, F. Alarab, P. C. Constantinou, V. Strocov, D. Usanov, W. R. Pudelko, R. González-Hernández, A. Birk Hellenes, Z. Jansa, H. Reichlová, Z. Šobáň, R. D. González Betancourt, P. Wadley, J. Sinova, D. Kriegner, J. Minár, J. H. Dil, and T. Jungwirth, Altermagnetic lifting of Kramers spin degeneracy, *Nature (London)* **626**, 517 (2024).
- [16] T. Osumi, S. Souma, T. Aoyama, K. Yamauchi, A. Honma, K. Nakayama, T. Takahashi, K. Ohgushi, and T. Sato, Observation of a giant band splitting in altermagnetic MnTe, *Phys. Rev. B* **109**, 115102 (2024).
- [17] G. Cuono, R. M. Sattigeri, J. Skolimowski, and C. Autieri, Orbital-selective altermagnetism and correlation-enhanced spin-splitting in strongly-correlated transition metal oxides, *Journal of Magnetism and Magnetic Materials* **586**, 171163 (2023).
- [18] C.-C. Wei, X. Li, S. Hatt, X. Huai, J. Liu, B. Singh, K.-M. Kim, R. M. Fernandes, P. Cardon, L. Zhao, T. T. Tran, B. A. Frandsen, K. S. Burch, F. Liu, and H. Ji,  $\text{La}_2\text{O}_3\text{Mn}_2\text{Se}_2$ : A correlated insulating layered *d*-wave altermagnet, *Phys. Rev. Mater.* **9**, 024402 (2025).
- [19] A. Damascelli, Z. Hussain, and Z.-X. Shen, Angle-resolved photoemission studies of the cuprate superconductors, *Rev. Mod. Phys.* **75**, 473 (2003).
- [20] P. A. Lee, N. Nagaosa, and X.-G. Wen, Doping a Mott insulator: Physics of high-temperature superconductivity, *Rev. Mod. Phys.* **78**, 17 (2006).
- [21] C. L. Kane, P. A. Lee, and N. Read, Motion of a single hole in a quantum antiferromagnet, *Phys. Rev. B* **39**, 6880 (1989).
- [22] S. Schmitt-Rink, C. M. Varma, and A. E. Ruckenstein, Spectral function of holes in a quantum antiferromagnet, *Phys. Rev. Lett.* **60**, 2793 (1988).
- [1] G. Martinez and P. Horsch, Spin polarons in the *t-j* model, *Phys. Rev. B* **44**, 317 (1991).
- [24] Y. Wang, K. Wohlfeld, B. Moritz, C. J. Jia, M. van Veenendaal, K. Wu, C.-C. Chen, and T. P. Devereaux, Origin of strong dispersion in Hubbard insulators, *Phys. Rev. B* **92**, 075119 (2015).
- [25] Y. Wang, Y. He, K. Wohlfeld, M. Hashimoto, E. W. Huang, D. Lu, S.-K. Mo, S. Komiya, C. Jia, B. Moritz, Z.-X. Shen, and T. P. Devereaux, Emergence of quasiparticles in a doped Mott insulator, *Communications Physics* **3**, 10.1038/s42005-020-00480-5 (2020).
- [26] B. Bacq-Labreuil, C. Fawaz, Y. Okazaki, Y. Obata, H. Cercellier, P. Le Fèvre, F. m. c. Bertran, D. Santos-Cottin, H. Yamamoto, I. Yamada, M. Azuma, K. Horiba, H. Kumigashira, M. d'Astuto, S. Biermann, and B. Lenz, Universal waterfall feature in cuprate superconductors: Evidence of a momentum-driven crossover, *Phys. Rev. Lett.* **134**, 016502 (2025).
- [27] F. Ronning, K. M. Shen, N. P. Armitage, A. Damascelli, D. H. Lu, Z.-X. Shen, L. L. Miller, and C. Kim, Anomalous high-energy dispersion in angle-resolved photoemission spectra from the insulating cuprate  $\text{Ca}_2\text{CuO}_2\text{Cl}_2$ , *Phys. Rev. B* **71**, 094518 (2005).
- [28] B. O. Wells, Z. X. Shen, A. Matsuura, D. M. King, M. A. Kastner, M. Greven, and R. J. Birgeneau, *e* versus *k* relations and many body effects in the model insulating copper oxide  $\text{Sr}_2\text{CuO}_2\text{Cl}_2$ , *Phys. Rev. Lett.* **74**, 964 (1995).
- [29] Kim, Jungho, Daghofer, M., Said, A. H., Gog, T., van den Brink, J., Khaliullin, G., and Kim, B. J., Excitonic quasipar-

- ticles in a spin-orbit Mott insulator, *Nature Communications* **5**, 4453 (2014).
- [30] L. Martinelli, K. Wohlfeld, J. Pelliciani, R. Arpaia, N. B. Brookes, D. Di Castro, M. G. Fernandez, M. Kang, Y. Krockenberger, K. Kummer, D. E. McNally, E. Paris, T. Schmitt, H. Yamamoto, A. Walters, K.-J. Zhou, L. Braicovich, R. Comin, M. M. Sala, T. P. Devereaux, M. Daghofer, and G. Ghiringhelli, Collective nature of orbital excitations in layered cuprates in the absence of apical oxygens, *Phys. Rev. Lett.* **132**, 066004 (2024).
- [31] G. Ji, M. Xu, L. H. Kendrick, C. S. Chiu, J. C. Brüggenjürgen, D. Greif, A. Bohrdt, F. Grusdt, E. Demler, M. Lebrat, and M. Greiner, Coupling a mobile hole to an antiferromagnetic spin background: Transient dynamics of a magnetic polaron, *Phys. Rev. X* **11**, 021022 (2021).
- [32] Koepsell, Joannis, Vijayan, Jayadev, Sompert, Pimonpan, Grusdt, Fabian, Hilker, Timon A., Demler, Eugene, Salomon, Guillaume, Bloch, Immanuel, and Gross, Christian, Imaging magnetic polarons in the doped Fermi-Hubbard model, *Nature* **572**, 358 (2019).
- [33] T. Müller, R. Thomale, S. Sachdev, and Y. Iqbal, Polaronic correlations from optimized ancilla wave functions for the fermi-hubbard model, *Proceedings of the National Academy of Sciences* **122**, 10.1073/pnas.2504261122 (2025).
- [34] S. Giuli, C. Mejuto-Zaera, and M. Capone, Altermagnetism from interaction-driven itinerant magnetism, *Phys. Rev. B* **111**, L020401 (2025).
- [35] F. Ferrari and R. Valentí, Altermagnetism on the Shastry-Sutherland lattice, *Phys. Rev. B* **110**, 205140 (2024).
- [36] J. a. A. Sobral, S. Mandal, and M. S. Scheurer, Fractionalized altermagnets: From neighboring and altermagnetic spin liquids to spin-symmetric band splitting, *Phys. Rev. Res.* **7**, 023152 (2025).
- [37] L. Šmejkal, A. Marmodoro, K.-H. Ahn, R. González-Hernández, I. Turek, S. Mankovsky, H. Ebert, S. W. D'Souza, O. c. v. Šipr, J. Sinova, and T. c. v. Jungwirth, Chiral magnons in altermagnetic RuO<sub>2</sub>, *Phys. Rev. Lett.* **131**, 256703 (2023).
- [38] Z. Liu, M. Ozeki, S. Asai, S. Itoh, and T. Masuda, Chiral split magnon in altermagnetic MnTe, *Phys. Rev. Lett.* **133**, 156702 (2024).
- [39] J. Fujioka, S. Miyasaka, and Y. Tokura, Orbital disordering and the metal-insulator transition with hole doping in perovskite-type vanadium oxides, *Phys. Rev. B* **72**, 024460 (2005).
- [40] S. Miyasaka, T. Okuda, and Y. Tokura, Critical behavior of metal-insulator transition in La<sub>1-x</sub>Sr<sub>x</sub>VO<sub>3</sub>, *Phys. Rev. Lett.* **85**, 5388 (2000).
- [41] X.-J. Zhang, E. Koch, and E. Pavarini, LaVO<sub>3</sub>: A true Kugel-Khomskii system, *Phys. Rev. B* **106**, 115110 (2022).
- [42] V. Leeb, A. Mook, L. Šmejkal, and J. Knolle, Spontaneous formation of altermagnetism from orbital ordering, *Phys. Rev. Lett.* **132**, 236701 (2024).
- [43] G. Martinez and P. Horsch, Spin polarons in the *t*-*J* model, *Phys. Rev. B* **44**, 317 (1991).
- [44] K. Wohlfeld, M. Daghofer, A. M. Oleś, and P. Horsch, Spectral properties of orbital polarons in Mott insulators, *Phys. Rev. B* **78**, 214423 (2008).
- [45] K. Wohlfeld, A. M. Oleś, and P. Horsch, Orbital induced string formation in the spin-orbital polarons, *Phys. Rev. B* **79**, 224433 (2009).
- [46] See the Supplemental Material at . . .
- [47] Z. Liu and E. Manousakis, Dynamical properties of a hole in a Heisenberg antiferromagnet, *Phys. Rev. B* **45**, 2425 (1992).
- [2] M. Potthoff, M. Aichhorn, and C. Dahnken, Variational cluster approach to correlated electron systems in low dimensions, *Phys. Rev. Lett.* **91**, 206402 (2003).
- [49] M. Daghofer, K. Wohlfeld, A. M. Oleś, E. Arrigoni, and P. Horsch, Absence of hole confinement in transition-metal oxides with orbital degeneracy, *Phys. Rev. Lett.* **100**, 066403 (2008).
- [50] X. Zhu, X. Huo, S. Feng, S.-B. Zhang, S. A. Yang, and H. Guo, Design of altermagnetic models from spin clusters, *Phys. Rev. Lett.* **134**, 166701 (2025).
- [51] D. Chakraborty and A. M. Black-Schaffer, Zero-field finite-momentum and field-induced superconductivity in altermagnets, *Phys. Rev. B* **110**, L060508 (2024).
- [52] S.-B. Zhang, L.-H. Hu, and T. Neupert, Finite-momentum cooper pairing in proximitized altermagnets, *Nature Communications* **15**, 1801 (2024).
- [53] S. Banerjee and M. S. Scheurer, Altermagnetic superconducting diode effect, *Phys. Rev. B* **110**, 024503 (2024).
- [54] Y. Li, V. Leeb, K. Wohlfeld, R. Valentí, and J. Knolle, *d*-Wave Magnetism in Cuprates from Oxygen Moments, *arXiv e-prints*, arXiv:2412.11922 (2024), arXiv:2412.11922 [cond-mat.str-el].
- [55] P. W. Anderson, Is there glue in cuprate superconductors?, *Science* **316**, 1705 (2007), <https://www.science.org/doi/pdf/10.1126/science.1140970>.
- [56] J. R. Schrieffer, X.-G. Wen, and S.-C. Zhang, Spin-bag mechanism of high-temperature superconductivity, *Phys. Rev. Lett.* **60**, 944 (1988).
- [57] X. Dong, L. D. Re, A. Toschi, and E. Gull, Mechanism of superconductivity in the Hubbard model at intermediate interaction strength, *PNAS* **119**, e2205048119 (2022).
- [58] Dong, Xinyang, Gull, Emanuel, and Millis, Andrew J., Quantifying the role of antiferromagnetic fluctuations in the superconductivity of the doped Hubbard model, *Nature Physics* **18**, 1293 (2022).
- [59] H. Yamase, Spin-fluctuation glue disfavors high-critical temperature of superconductivity?, *New Journal of Physics* **25**, 083049 (2023).
- [60] L. Lanzini, P. Das, and M. Knap (2025)

## SUPPLEMENTAL MATERIAL: ALTERMAGNETIC POLARONS

This supplemental material contains details on the self-consistent Born approximation (SCBA) and the variational cluster approximation, as well as on the  $t_{2g}$  Hamiltonian base on  $\text{LaVO}_3$ . We additionally present one-particle spectra of the Hubbard model on the Shastry-Sutherland lattice to complement the checkerboard lattice discussed in the main text.

### Self-consistent Born approximation

This section contains for completeness the equations used in obtaining the results with SCBA presented in the main text.

Equation (3) of the main text is obtained via linearised spin wave, Fourier and Bogoliubov transformations [S1]. After Fourier transform, a spin flip away from the Néel reference state is denoted by operators

$$a_{\mathbf{k}} = u_{\mathbf{k}}\alpha_{\mathbf{k}} - v_{\mathbf{k}}\beta_{-\mathbf{k}}^{\dagger} \quad (\text{S1})$$

$$b_{\mathbf{k}} = u_{\mathbf{k}}\beta_{\mathbf{k}} - v_{\mathbf{k}}\alpha_{-\mathbf{k}}^{\dagger}, \quad (\text{S2})$$

where  $a_{\mathbf{k}}$  and  $b_{\mathbf{k}}$  refer to a spin flip on  $A$  and  $B$  sublattices, resp. Coefficients  $u_{\mathbf{k}}$  and  $v_{\mathbf{k}}$  are chosen to diagonalize the magnon Hamiltonian

$$(a_{\mathbf{k}}^{\dagger}, b_{\mathbf{k}}) \begin{pmatrix} h_A & h_{AB} \\ h_{AB} & h_B \end{pmatrix} \begin{pmatrix} a_{-\mathbf{k}} \\ b_{-\mathbf{k}}^{\dagger} \end{pmatrix} = \omega_{\alpha,\mathbf{k}} \alpha_{\mathbf{k}}^{\dagger} \alpha_{\mathbf{k}} + \omega_{\beta,\mathbf{k}} \beta_{\mathbf{k}}^{\dagger} \beta_{\mathbf{k}} \quad (\text{S3})$$

with

$$h_{A/B} = 2J - J' + J' \cos k_{a/b}, \quad h_{AB} = 2J\gamma_{\mathbf{k}}, \quad (\text{S4})$$

$$\gamma_{\mathbf{k}} = \frac{1}{2} \left( \cos \frac{k_a + k_b}{2} + \cos \frac{k_a - k_b}{2} \right) = \frac{1}{2} (\cos q_x + \cos q_y). \quad (\text{S5})$$

Momenta  $\mathbf{k} = (k_a, k_b)$  refer to the first Brillouin zone of the checkerboard lattice with its two-site unit cell, momenta  $\mathbf{q} = (q_x, q_y)$  would correspond to a square lattice with a single-site unit cell. One then finds

$$u_{\mathbf{k}} = \cosh \theta, \quad v_{\mathbf{k}} = \sinh \theta, \quad \theta = \frac{1}{2} \text{atanh} \left( \frac{2h_{AB}}{h_A + h_B} \right) \quad (\text{S6})$$

and

$$\omega_{\alpha/\beta,\mathbf{k}} = h_{A/B} v_{\mathbf{k}}^2 + h_{B/A} u_{\mathbf{k}}^2 - 2u_{\mathbf{k}} v_{\mathbf{k}} h_{AB}. \quad (\text{S7})$$

This completes the transformation of the spin Hamiltonian (2) into the Eq. (3) of the main text.

Next, using successive slave-fermion, Fourier and Bogoliubov transformations, see [S1] for details, we express kinetic energy, Eq. (1) of the main text in terms of hole  $h$  and, if needed, magnon  $\alpha, \beta$  creation and annihilation operators. NNN electron hopping within a sublattice leads to hole moving without coupling to magnons and reads

$$\tilde{H}_{t,2} = 2t' \sum_{\mathbf{k}} \left( \cos k_a h_{\mathbf{k},A}^{\dagger} h_{\mathbf{k},A} + \cos k_b h_{\mathbf{k},B}^{\dagger} h_{\mathbf{k},B} \right), \quad (\text{S8})$$

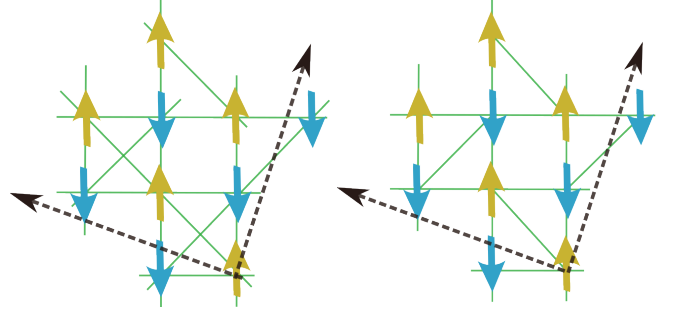


FIG. S1. Ten-site clusters that were used in the variational cluster approximation for the Hubbard model on (a) the checkerboard and (b) the Shastry-Sutherland lattices. Black dashed arrows indicate the lattice vectors of the supercell, i.e., how the clusters are connected when obtaining the Green's function of the lattice.

where  $h_{\mathbf{k},\alpha}^{\dagger}$  ( $h_{\mathbf{k},\alpha}$ ) creates (annihilates) a hole with momentum  $\mathbf{k}$  on sublattice  $\alpha = A, B$ . NN hopping between sublattices in contrast creates or annihilates magnons and thus couples hole motion and magnons:

$$\tilde{H}_t = \frac{zt}{\sqrt{N_u}} \sum_{\mathbf{k},\mathbf{k}'} M_{\mathbf{k},\mathbf{k}'} \left( h_{\mathbf{k},A}^{\dagger} h_{\mathbf{k}-\mathbf{k}',B} \alpha_{\mathbf{k}'} + h_{\mathbf{k},B}^{\dagger} h_{\mathbf{k}-\mathbf{k}',A} \beta_{\mathbf{k}'} \right) + \text{H.c.}, \quad (\text{S9})$$

with  $z = 4$  NN bonds per site and the number  $N_u$  of two-site unit cells.  $M_{\mathbf{k},\mathbf{k}'} = (-v_{\mathbf{k}'}\gamma_{\mathbf{k}} + u_{\mathbf{k}'}\gamma_{\mathbf{k}-\mathbf{k}'})$  depends on the constants  $u_{\mathbf{k}'}$  and  $v_{\mathbf{k}'}$  arising in the Bogoliubov transformation (S6) above. Equations (S8) and (S9) are the one-hole approximation of the kinetic energy (1) of the main text.

We are here interested in spectral densities obtained from sublattice-dependent hole Green's functions

$$G^{\alpha}(\mathbf{k}, \omega) = \langle \phi_0 | h_{\mathbf{k},\alpha} \frac{1}{\omega - (\tilde{H} - E_0) + i\delta} h_{\mathbf{k},\alpha}^{\dagger} | \phi_0 \rangle, \quad (\text{S10})$$

where  $\tilde{H} = \tilde{H}_J + \tilde{H}_t + \tilde{H}_{t,2}$  is the approximated one-hole Hamiltonian,  $\alpha = A, B$  is the sublattice index, and the ground state  $|\phi_0\rangle$  is the undoped linear-spin-wave ground state. Dyson equation and self energy of the main text then complete the SCBA for the sublattice-dependent Green's functions. Alternating magnetic order ties spin character to sublattice, however, quantum fluctuations reduce the correlation so that

$$G^{\dagger}(\mathbf{k}, \omega) = G^A(\mathbf{k}, \omega) + \left( \frac{1}{N_u} \sum_{\mathbf{k}} v_{\mathbf{k}}^2 \right) (G^B(\mathbf{k}, \omega) - G^A(\mathbf{k}, \omega)) \quad (\text{S11})$$

and analogously for  $G^{\downarrow}(\mathbf{k}, \omega)$ . These corrections can become quite substantial for large  $J'$ .

### Variational Cluster approximation

In addition to the SCBA applied to the  $t$ - $J$  model we also study a Hubbard model on the checkerboard lattice with the



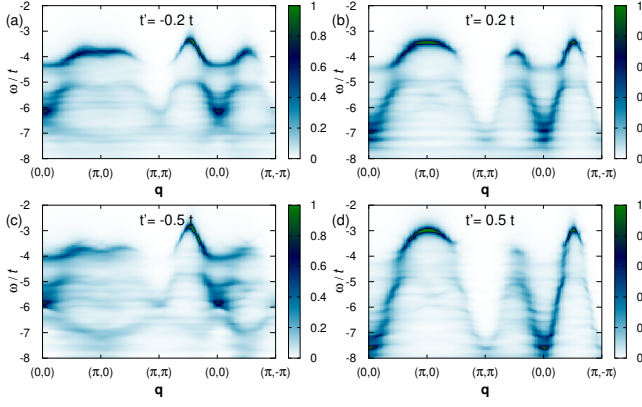


FIG. S2. One-particle spectral density for spin up, obtained with VCA for the checkerboard model with  $U = 10 t$  in the AF state optimizing the grand potential for (a)  $t' = -0.2 t$ , (b)  $t' = 0.2 t$ , (c)  $t' = -0.5 t$ , and (d)  $t' = 0.5 t$ .

variational cluster approximation (VCA) [S2, S3]. As in cluster perturbation theory, the self energy  $\Sigma$  of the system is replaced by the self energy  $\Sigma_{\text{Cl}}$  of a small cluster, which is in turn extracted from the Green's function  $G_{\text{Cl}}$  of the cluster. The cluster self energy  $\Sigma_{\text{Cl}}$  is then combined with the non-interacting Green's function  $G_0^{-1}$  of a lattice to yield an approximation

$$G = (G_0^{-1} - \Sigma)^{-1} \approx (G_0^{-1} - \Sigma_{\text{Cl}})^{-1} \quad (\text{S12})$$

of the full lattice Green's function. We use here a ten-site cluster, as it is more symmetric than eight- or twelve-site clusters and the next highly symmetric cluster (sixteen sites) would be numerically rather demanding.

In the VCA, the self energy is further optimized by finding a stationary point of the grand potential w.r.t. one-particle parameters of the Hamiltonian. The grand canonical potential  $\Omega$  of the lattice system can be written as

$$\Omega = \Omega_{\text{Cl}} + Tr \ln [G_0^{-1} - \Sigma_{\text{Cl}}]^{-1} - Tr \ln (-G_{\text{Cl}}), \quad (\text{S13})$$

where  $\Omega_{\text{Cl}}$  is the grand canonical potential of the cluster [S4, S5]. In our case, we find that the self energy calculated with an additional small staggered magnetic field lowers the system's energy. However, it must be emphasized that the calculated observables (e.g. the spectral density) are obtained using the 'original' Hamiltonian, i.e., the staggered field is not included in the non-interacting lattice Green's function  $G_0^{-1}$ .

Figure S2 shows the one-particle spectra obtained in the AF state optimizing the grand potential at half filling. The onsite interaction  $U$  was here set to  $10 t$ , giving  $J = \frac{4t^2}{U} = 0.4 t$  as in the main text, and second-neighbor hopping to  $t' = \pm 0.5 t$  resp.  $t' = \pm 0.2 t$ . The relevant momenta for altermagnetism are  $\mathbf{q} = (\frac{\pi}{2}, \pm \frac{\pi}{2})$  resp.  $\mathbf{k} = (0, \pi)$  and  $\mathbf{k} = (\pi, 0)$ . While the spectrum for  $t' = \pm 0.2 t$  shows one peak for each spin projection, one (closer to the Fermi level) has much higher weight than the other and is also sharper. For the larger  $t' = \pm 0.5 t$ , only one coherent QP peak with a clear spin polarization

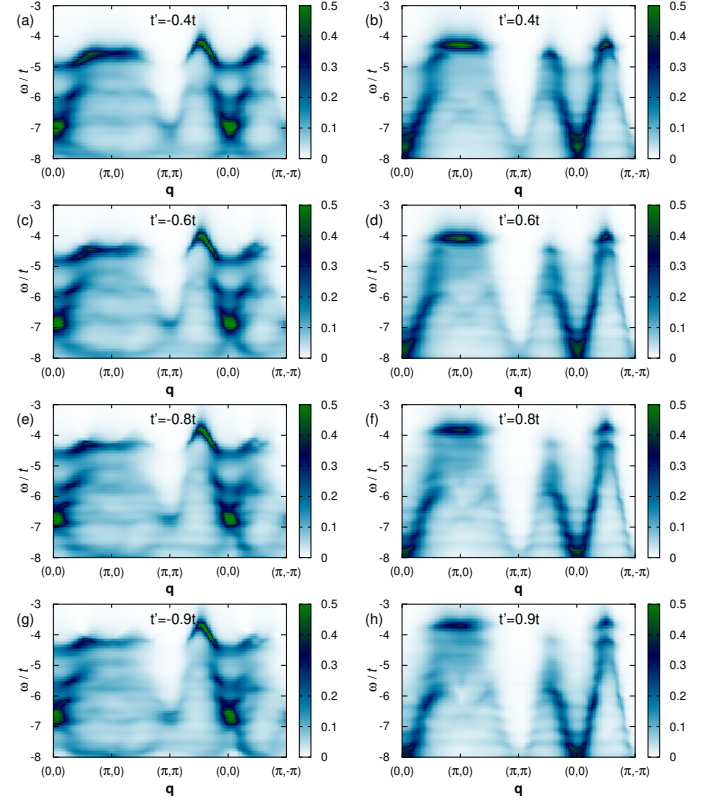


FIG. S3. One-particle spectral density for spin up, obtained with VCA for the Hubbard model on the Shastry-Sutherland lattice for  $t = 1$ ,  $U = 12 t$  and various positive or negative  $t'$ . The system here prefers the AF state.

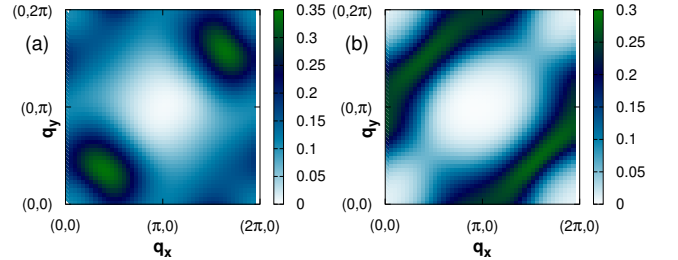


FIG. S4. Energy-integrated one-particle spectral density for spin up, obtained with VCA for the Hubbard model on the Shastry-Sutherland lattice for  $t = 1$ ,  $U = 12 t$  and (a)  $t' = -0.8 t$ , (b)  $t' = 0.8 t$ . Energies were integrated over  $-5 \leq \omega \leq -3$  in (a) and  $-4.7 \leq \omega \leq -3.0$  in (b).

around these momenta is seen, as in the SCBA results of the main text.

### VCA for the Shastry-Sutherland model

In order to go beyond the checkerboard model, we also look at the Shastry-Sutherland lattice. Compared to the checkerboard model of the main text, every second 'diagonal' hopping is here missing. Denoting sites with coordinate pairs



$(i_x, i_y)$ , the kinetic energy can be written as

$$H_{\text{sh-su}} = -t \sum_{\langle i,j \rangle, \sigma} c_{i,\sigma}^\dagger c_{j,\sigma} \quad (\text{S14})$$

$$-t' \sum_{i_x, i_y, \sigma} \left( c_{(i_x+1, i_y+1), \sigma}^\dagger c_{(i_x, i_y), \sigma} + \text{H.c.} \right)$$

$$-t' \sum_{i_x, i_y, \sigma} \left( c_{(i_x-1, i_y), \sigma}^\dagger c_{(i_x, i_y-1), \sigma} + \text{H.c.} \right).$$

Due to its four-site unit cell, any SCBA treatment would also have to be based on four magnon flavors, none of which could be allowed to cross lines. This excludes processes where a spin flip created in the sublattice with  $i_x, i_y$  both even is annihilated in sublattice  $i_x, i_y$  both odd, even though this would be physically allowed, because both sublattices have the same spin. The non-crossing approximation inherent in the SCBA is here thus harder to justify, and we instead use the VCA to look at the Hubbard model given by (S14) and onsite Coulomb repulsion.

$$H_U = U \sum_{(i_x, i_y)} n_{(i_x, i_y), \uparrow} n_{(i_x, i_y), \downarrow}. \quad (\text{S15})$$

Spin-resolved spectra are shown in Fig. S3. While two spin-split bands may be identified at smaller  $|t'| \lesssim 0.6 t$ , larger values of  $|t'|$  again rather suggest a coherent QP with spin-momentum locking coming together with more incoherent weight of opposite spin. This is supported by the energy-integrated spectral weight shown in Fig. S4 for  $t' = \pm 0.8 t$ . The energy window chosen for the integration captures both the dominant QP peak as well as the top features at different momenta, but remains clearly spin-momentum locked.

### Details of the $t_{2g}$ Hamiltonian

Finally, we also looked at a three-orbital model for  $t_{2g}$  orbitals, based on  $\text{LaVO}_3$ . The onsite interactions are here taken

$$H_{\text{int}} = U \sum_{i, \alpha} n_{i\alpha\uparrow} n_{i\alpha\downarrow} + \frac{U'}{2} \sum_{i, \sigma} \sum_{\alpha \neq \beta} n_{i\alpha\sigma} n_{i\beta\bar{\sigma}} \quad (\text{S16})$$

$$+ \frac{1}{2} (U' - J_H) \sum_{i, \sigma} \sum_{\alpha \neq \beta} n_{i\alpha\sigma} n_{i\beta\sigma} \quad (\text{S17})$$

$$- J_H \sum_{i, \alpha \neq \beta} (c_{i\alpha\uparrow}^\dagger c_{i\alpha\downarrow} c_{i\beta\downarrow}^\dagger c_{i\beta\uparrow}) \quad (\text{S18})$$

$$+ J_H \sum_{i, \alpha \neq \beta} (c_{i\alpha\uparrow}^\dagger c_{i\alpha\downarrow}^\dagger c_{i\beta\downarrow} c_{i\beta\uparrow}) \quad (\text{S19})$$

with Coulomb interaction  $U$ ,  $U'$  and Hund's coupling  $J_H$  connected via  $U' = U - 2J_H$ . We use here also NN hopping  $t \approx 0.2 \text{ eV}$  as unit of energy. Remaining parameters are  $\Delta = -0.5 t$  (favoring  $xy$  occupation),  $U = 14 t$  and  $J_H = 2 t$ . The VCA was here based on a plaquette of size  $2 \times 2$  sites.

- 
- [S1] G. Martinez and P. Horsch, Spin polarons in the  $t$ - $j$  model, [Phys. Rev. B \*\*44\*\*, 317 \(1991\)](#).
  - [S2] M. Potthoff, M. Aichhorn, and C. Dahnken, Variational cluster approach to correlated electron systems in low dimensions, [Phys. Rev. Lett. \*\*91\*\*, 206402 \(2003\)](#).
  - [S3] M. Aichhorn, H. G. Evertz, W. von der Linden, and M. Potthoff, Charge ordering in extended Hubbard models: Variational cluster approach, [Phys. Rev. B \*\*70\*\*, 235107 \(2004\)](#).
  - [S4] M. Potthoff, Self-energy-functional approach: Analytical results and the Mott-Hubbard transition, [The European Physical Journal B - Condensed Matter and Complex Systems \*\*36\*\*, 335 \(2003\)](#).
  - [S5] M. Aichhorn, E. Arrigoni, M. Potthoff, and W. Hanke, Antiferromagnetic to superconducting phase transition in the hole- and electron-doped Hubbard model at zero temperature, [Phys. Rev. B \*\*74\*\*, 024508 \(2006\)](#).